An Analog Light Scattering Experiment of Hexagonal Icelike Particles. Part I: Experimental Apparatus and Test Measurements

BRIAN BARKEY AND K. N. LIOU*

Department of Meteorology/CARSS, University of Utah, Salt Lake City, Utah

WERNER GELLERMAN AND PIERRE SOKOLSKY

Department of Physics, University of Utah, Salt Lake City, Utah

(Manuscript received 13 June 1997, in final form 30 April 1998)

ABSTRACT

An experimental apparatus to measure the scattering properties of hexagonal icelike particles in the analog manner at the helium neon laser wavelength of 0.633 μm has been designed and built. The instrument consists of an array of 36 highly sensitive and linear photodiode detectors that are positioned to measure the light between the scattering angles of 2.8° and 177.2° in approximately 2.5° increments and at any desired azimuthal angle. This array is calibrated such that the retrieved light signals are corrected to the actual light seen by the detectors to within approximately 6% at all applicable scattering and azimuthal angles. A system of electro-mechanical positioners places the sample at the desired and known position. A glass sphere and a glass fiber configured to scatter light like an infinite cylinder was used to test the operational effectiveness and calibration of the experimental apparatus. The phase functions for the parallel and perpendicular components determined from the experimental results match closely with the results computed from Mie theory.

1. Introduction

A number of different experimental studies have been carried out in the past to investigate the scattering behaviors of nonspherical particles. These studies can be generally divided into two groups: optical and microwave. The optical method has been used to study the scattering properties of ice crystals in cloud chambers (Huffman and Thursby 1969; Dugin et al. 1977; Sassen and Liou 1979a,b; Kuik 1992). A direct comparison of the scattering results determined from cloud experiments to theory cannot be performed exactly because the contribution from each scattering particle cannot be separated and the exact orientation and position of the ice crystals are not known. In addition, there is the problem of multiple scattering in these experiments. Moreover, the generation of desirable ice crystal shapes and sizes in cold chambers is extremely difficult, particularly in connection with optical experiments.

Pluchino (1986, 1987) examined the light scattered from an electrostatically balanced and isolated ice crystal. Due to the nature of this study, the exact size, shape, and orientation of the crystal was unknown. Also, the crystal position oscillated at a low frequency. The microwave method has been carried out by means of analog experiments by a number of researchers: Zerull et al. (1993) studied interstellar dust particle shapes; Hage et al. (1991) investigated cubic shapes; Schuerman et al. (1981) and Lind et al. (1965) examined various ellipsoids; and Greenberg et al. (1960) studied cylinders. Moreover, Fuller et al. (1994) measured the scattering properties of a hexagonal crystal in the microwave region. Due to the size of the incident wavelength (λ = 3.18 cm) the facilities used for these experiments are extremely large, and the applicable size parameter ($2\pi a/\lambda$, where a is the length of the semimajor axis and λ is the wavelength) is normally less than 10.

The present study is the first known experiment to allow the analog investigation of the scattering properties of nonspherical particles similar to ice crystals in the geometric optics region. The results of this experiment can be directly compared to theoretical calculations because the size, shape, spatial orientation, and optical properties of the scattering sample are known. This analog approach requires that we measure the scattering parameters of nonspherical particles at both the scattering and azimuthal angles. The experimental results will be used to cross-check the theoretical results

* Current affiliation: Department of Atmospheric Sciences, University of California, Los Angeles, Los Angeles, California.

Corresponding author address: Dr. Brian Barkey, 201 JFB, Department of Physics, University of Utah, Salt Lake City, UT 84112. E-mail: barkey@mail.physics.utah.edu

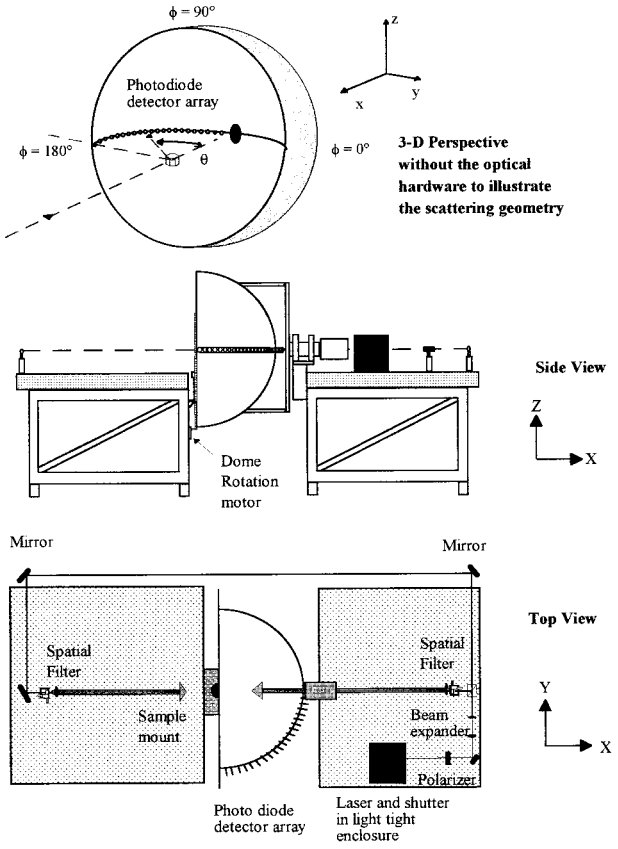

FIG. 1. Three-dimensional view, side view, and top view of the experimental apparatus.

simulated from the geometric ray tracing methods developed by Takano and Liou (1989, 1995). The importance of the scattering properties of nonspherical ice crystals for applications to remote sensing and climate studies has been articulated in Liou and Takano (1994) and Liou (1992).

The present paper is the first of a two-part report in which the physical description of the experimental apparatus is presented. The design of this experiment requires the development of novel methods to collect and analyze the retrieved scattering signals. A sphere and an infinite cylinder are used to show the effectiveness of the equipment. In the second part, the scattering properties of several hexagonal crystals, including columns, plates, aggregates, and crystals with rough surfaces, made out of sodium fluoride (NaF), that have optical properties very close to that of ice are presented.

2. Description of the experimental apparatus

The experimental setup consists of 36 photodiode detector–amplifier units (PDU) mounted in a linear array on a 0.635-cm-thick plastic half dome that averages 115 cm in diameter. This dome is mounted between two 122 cm^2 optical tables as shown in Fig. 1 (top and side views). The dome is mounted on a gimbal with its rotating axis in the horizontal scattering plane that is defined to be 15 cm above the optical table surface. The dome rotates about the axis defined by the incident light direction, which is the line running along the center of the tables in the horizontal scattering plane. An aluminum frame prevents distortion of the PDU array as the dome is rotated. There is a 2.5-cm-diameter hole in the center of the dome and through the axis of the gimbal axis shaft to allow laser light to enter the experiment from the reverse direction.

The plane of scattering detection is defined by the azimuthal position of the PDU array as shown in Fig. 1 (3D perspective). By rotating the dome, the PDU array detection plane can be properly positioned to measure the light scattered into any desired azimuthal angle, which is designated as ϕ. The small sample platform is located approximately 48 cm below the center of the dome to which translators, rotators, and other positioning equipment can be mounted as each experiment requires. A small reversible A/C motor geared to rotate at 4 rpm turns the dome via a rack and pinion gear arrangement mounted to the rim of the dome, which rotates the dome at a speed of 0.063 rotations per minute. This motor is controlled by the computer and because of the slow speed of dome rotation, the azimuthal position is determined by simply controlling the time of the motor operation. The measured precision ($\Delta\phi$) of the dome azimuthal position with the computer-controlled interface throughout its range of motion is better than 0.4%.

The individual detector location in the dome determines the scattering angle, designated as θ. The 36 detectors span the angular extent of $\theta = 2.8°$ to 89.6° in increments that vary between 2.25° and 2.5°. The measured angular positions of these detectors are accurate to ± 0.2. The inside of the dome is painted a flat black, as are all other surfaces that could reflect light into the detectors. The whole apparatus is inside a black felt enclosure and light traps are placed at points of strong intensity to reduce the effect of stray reflections. Despite these precautions, most measurements have some level of light contamination due to stray reflections.

The output of a helium neon laser is expanded to a beam diameter of approximately 5 mm and then directed with mirrors around the dome for forward scattering measurements or through the center of the dome for reverse measurements as shown in Fig. 1. The polarization plane of the laser is oriented at an angle of 45° to the horizontal scattering plane. A Glan–Thompson polarizer placed in a rotating mount with a vernier dial is used to select either the parallel or perpendicular polarization component of the laser beam for use in the experiment. A depolarizer, optimized for the helium neon wavelength, is used to unpolarize the incident light when needed. The scattered light intensity is sensed by silicon photodiode detectors (Hammamatsu S1226-44bk) with large sensing areas ($\simeq 1/3$ cm^2) connected

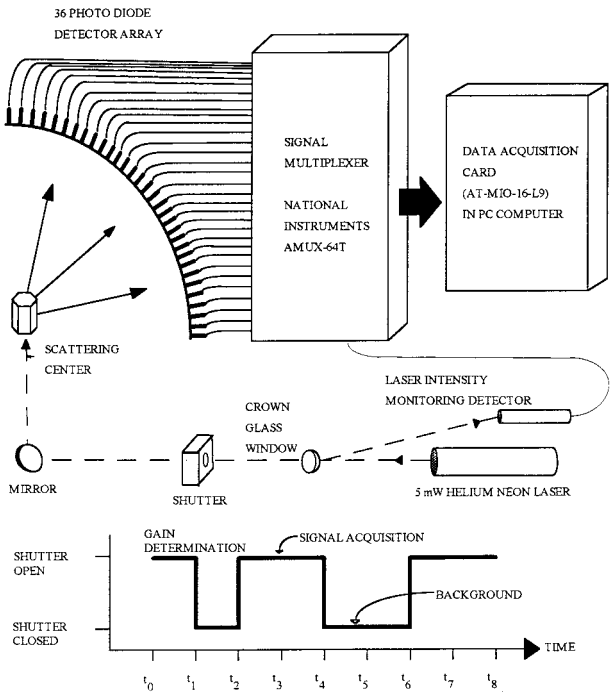

FIG. 2. A functional block diagram of the data acquisition system is seen in the upper part of this diagram. The lower plot is a time sequence of the signal acquisition method used in the experiment.

to high gain, low noise operational amplifiers (Burr-Brown OPA128). The detector circuit housing is mounted onto an aluminum frame, which is then mounted to the plastic dome with epoxy resin. Only the photodiode detector sensing area protrudes into the dome through a 14-mm-diameter hole such that the glass window of the detector is placed flush with the inside of the dome.

3. Calibration and signal acquisition

The photodiode and signal amplification circuit have been chosen for their wide dynamic range, linear response characteristics, and high sensitivity (Eppeldauer and Hardis 1991), but these characteristics can vary from photodiode to photodiode due to manufacturing and installation differences. The purpose of the calibration is to determine these photodiode characteristics and, if necessary, compensate for them.

A functional diagram of the data acquisition and signal analysis system is shown in Fig. 2. The 36 PDU array produce signals, which vary from 0 to 10 volts DC, proportional to the scattered light that falls on each detector's active sensing area. The voltage signal from each PDU is directed, via shielded cables, to a signal multiplexer (National Instruments AMUX-64T) that routes these signals to a data acquisition card (National Instruments AT-MIO-16-L9) in a personal computer (Gateway 386/25SX). The data acquisition card includes a voltmeter and a 12-bit analog to digital converter that converts the voltage signals to digital signals for use by the computer. This acquisition card can amplify the input voltage signals by 1, 10, 100, or 500 times and can discriminate voltage signals from 4.88 millivolts to 9.76 μvolts depending on the input gain. For instance, at a gain of 1, the maximum voltage detectable is 10 volts, but voltages are discriminated at increments of 4.88 millivolts. At higher input gain levels, the maximum detectable signal is reduced, but the level of signal discrimination is increased; that is, at an input gain of 500, the maximum signal is 0.02 volts, but the signals are discriminated in increments of 9.76 μvolts. The voltage levels of any selected channel can be measured at a rate of up to 100 000 samples per second. The multiplexing, gain selection, and voltage measurements are controlled by software written for this application in the proprietary development environment provided by National Instruments (LabWindows version 2.3). As shown in Fig. 2, the laser intensity is constantly monitored by reflecting a small percentage of the laser beam intensity to a PDU by a crown glass window to be used as a reference to eliminate the effects of laser intensity drift as explained later.

The computer controls an electro-mechanical shutter (UniBlitz Model D122) that switches the laser light from the 5-mW polarized laser into the experiment. This allows us to discriminate the background light levels from those produced by the laser light as shown in the bottom part of Fig. 2. First the shutter is opened and a voltage reading is taken from the 36 PDUs installed in the dome ($t = t_0$ to $t = t_1$ in the lower plot of Fig. 2). These voltages are used to determine the gain settings that maximize acquisition sensitivity; that is, a high gain setting of 500 is selected for voltages below 20 millivolts to take advantage of the 9.76-μvolt voltage sensitivity at this gain level. The shutter is then closed and voltage readings are taken to set gain levels for background light level acquisition (t_1 to t_2 in Fig. 2). Simultaneously, a voltage reading of the laser power monitoring detector is made. Next, 50 voltage readings of each of the 36 PDUs are taken at 20 000 points per second with the shutter opened (t_2 to t_4 in Fig. 2). The shutter is then closed and 50 more voltage readings are taken from each PDU in the array to measure the background light level in the experiment (t_4 to t_6 in Fig. 2). From these measurements, the scattered light signal to laser intensity monitor ratio is determined by

$$S_j = \left(\sum_{i=1}^{50} \frac{V_{soj}(i)}{V_{pm}} - \sum_{i=1}^{50} \frac{V_{scj}(i)}{V_{pm}} \right) \Big/ 50, \qquad (1)$$

where S_j is the signal returned for each detector j; $V_{scj}(i)$ is the ith measurement of the voltage from detector j with the shutter open, hence the laser light incident on the experiment; $V_{scj}(i)$ is the ith measurement of the voltage from detector j with the shutter closed (background light level); and V_{pm} is the voltage returned by the laser intensity monitoring detector. This signal acquisition process takes approximately 10 s. These sig-

nals are the ratio of the detector voltages to the voltage produced by the detector monitoring the laser output power, which compensates for the fluctuations in the laser power output.

The variability of this retrieved signal is dependent on the level of background light levels and on the level of the retrieved signal. To increase the precision of each signal measurement, the data acquisition process (t_2 to t_6 in Fig. 2) is repeated. The dynamic range of this acquisition method with a measured precision of less than 2% is limited to the upper 4 decades. At lower intensities background noise levels increase the variability of the retrieved signal to over 5%.

These detectors have been shown to be linear over 8 decades (Budde 1979). In this experiment and with the described acquisition scheme, the detectors have been found to respond linearly to the incident light intensity over a dynamic range of over three decades within 2%–3%. The loss of linearity at lower intensities is due to background light influencing the retrieved light signal. The response characteristics of each detector were measured and then adjusted such that the outputs of each detector are consistent with each other. The calibrated output of the PDU array has been measured and its response to an isotropic point source placed at the dome center is correct to within 6% over three decades throughout the azimuthal range of the array. A detailed description of this response measurement and calibration method is described in Barkey (1997). For measurements in the horizontal two-dimensional plane, phase functions are produced by measuring the scattering intensity as a function of angle in both the forward and reverse directions.

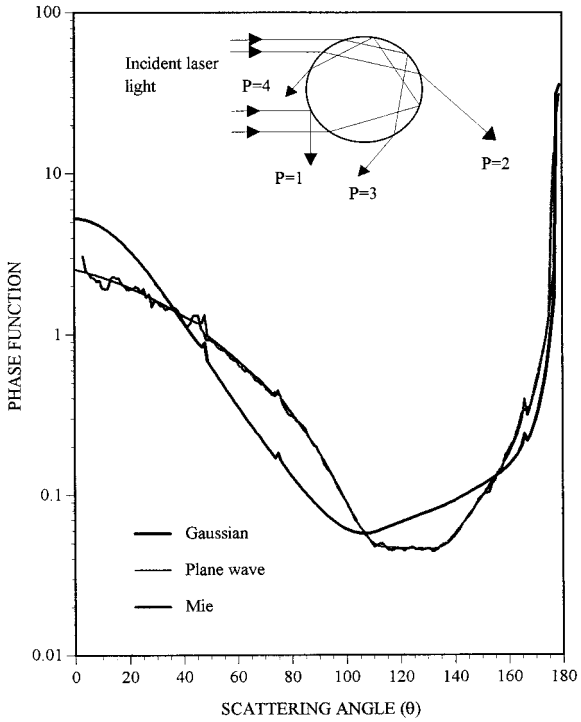

FIG. 3. The effect of the Gaussian intensity distribution of the laser beam on the angular scattering profile of a sphere as calculated via ray tracing methods. Also shown is the exact Mie theory result for incident plane wave light.

4. General measurement considerations

A system of electro-mechanical positioners allows the sample to be precisely placed in three directions, rotationally about the vertical z axis, horizontally along the x axis, and vertically about the z axis. The sample positioning equipment is designed to be at least 15 cm from the scattering center and painted black to reduce the effect of spurious reflections.

The light source is a Uniphase model 1105P 5-milliwatt linearly polarized helium neon laser that produces light at a wavelength of 0.633 m. This light is coherent and monochromatic, and it has a minimum polarization ratio of 500:1. The laser operates in the Gaussian TEM_{00} mode; that is, the radial profile of the laser beam is determined by

$$I(r) = I_0 e^{-2r^2/w^4}, \tag{2}$$

where $I(r)$ is the intensity of the laser light at the beam radius r, I_0 is the laser beam intensity at the center of the laser beam, and w is the laser beam waist, or the laser beam radius at which the laser beam intensity falls to a value $1/e^2$ of the axial value.

This laser beam does not present a constant intensity wave front to the sample, as is assumed in most models that predict the characteristics of the scattered light. As such, we have two options to circumvent this discrepancy: either use a Gaussian beam profile in our theoretical modeling or configure the laser beam to reduce or, if possible, eliminate the effects of the Gaussian intensity distribution. Ray tracing methods lend themselves easily to inhomogenous incident light intensity profiles. In Fig. 3, the expected scattering behavior for unpolarized helium neon light scattered from a 5-mm glass sphere with both an incident plane wave and with a TEM_{00} Gaussian beam with a waist size of 2.37 mm, is plotted. The effects of diffraction are not included in these calculations. Compared to plane wave light, incident light with a Gaussian profile increases the forward scattering and reduces the side scattering. Ignoring the effects of diffraction, this is because the light scattered into the forward direction is mainly due to the light that undergoes two refractions or P = 2 in the drawing at the top of Fig. 3. Light incident about the center of the sphere produces most of the intensity in the forward direction and is increased in the Gaussian case. Light that is side scattered is mainly due to the light that is reflected (P = 1 in Fig. 3), which is reduced under the Gaussian condition. External reflection (P = 1) produces most of the energy for light scattered into the reverse direction; the contribution from this case is reduced under the Gaussian condition. The angular scat-

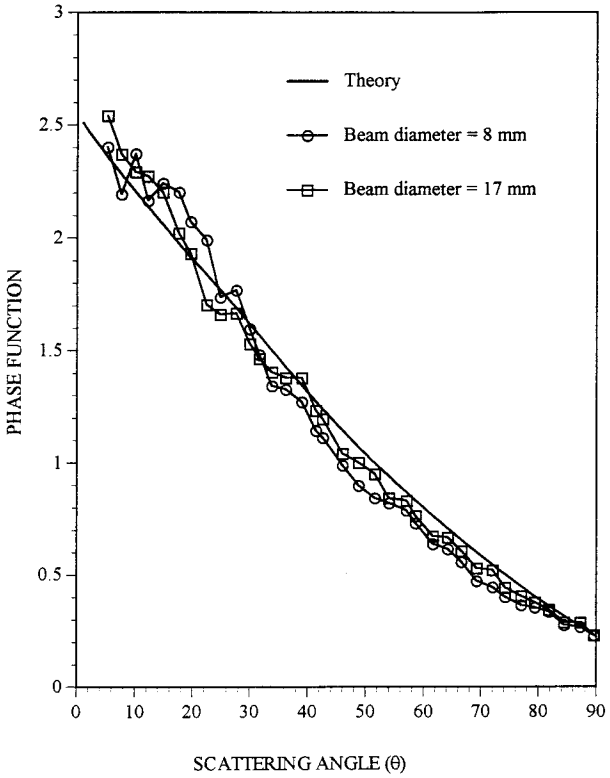

FIG. 4. Effect of variation of the waist size of the incident laser beam on the light scattered from a 5-mm glass sphere.

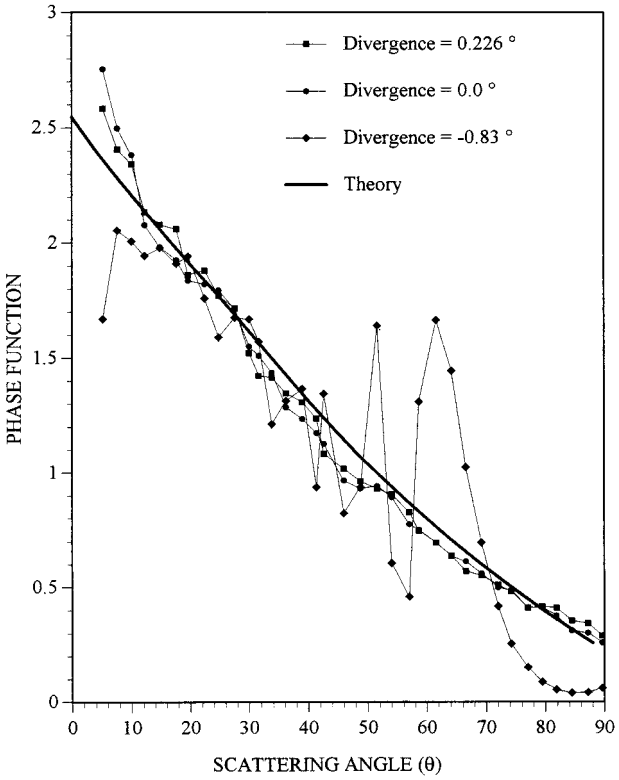

FIG. 5. Effect of the divergence of the incident laser beam on the light scattering characteristics of a 5-mm glass sphere.

tering position of other features, that is, rainbow peaks, do not change under the Gaussian condition.

The Mie theory expectations of a helium neon laser beam incident on the 5-mm glass sphere is also plotted in Fig. 3. This curve does not include the Gaussian beam correction, hence it closely follows the non-Gaussian ray tracing expectations. Each detector integrates the received intensity over its active sensing area, 1/3 cm^2 or a solid angle of 1×10^{-4} steradians or an angular extent of 0.3°. To reflect the larger sensing angle, the Mie theory results are smoothed by averaging the calculated results of several size parameters and then further smoothed by a running average of adjacent points that are determined at intervals less than 0.5° apart. Since the optical characteristics and the spatial position of our scattering sample are well known, the exact theoretically expected scattering pattern can be determined for each incident light configuration, hence a simple least squares fitting method is used to fit experimental results to theoretical expectations.

a. Sphere

A sphere is used to determine the effect of laser beam collimation, laser beam waist size, and the sample pedestal on the scattering parameters obtained by this experimental setup. The glass sphere used in these studies is 5 mm in diameter (± 1 μm), has an index of refraction of 1.844 91, has negligible absorption, and has a sphericity corrected to a quarter-wavelength at the helium neon wavelength.

Figure 4 shows the effect of changing the laser beam waist size on the forward scattering pattern of the 5-mm glass sphere. The theoretical expectation plotted in Fig. 4 does not include the effects of the Gaussian laser beam. We assumed that the beam radius, or the radial diameter at which the laser intensity falls to $1/e^2$ of the center axial intensity, can be determined by the radius of the visual ''spot'' of the spatially filtered laser beam. This beamwidth measurement is estimated to be 90% accurate. A wider beam more closely approaches the flat plane wave condition, hence its scattering pattern is closer to the theoretical result. The laser beam size is limited by the optics as a larger beam interferes with the lens holder assembly, producing diffraction rings that affect the scattering pattern. Also, in all of these forward scattering measurements, the laser beam saturates the detector placed at 2.5°, which is not included in the plotted results. A beam wider than 20 mm in diameter would affect the detector placed at 5°. Similar experiments on the effect of the beam size in the reverse direction are similar, though less dramatic.

The effect on the divergence or convergence of the incident laser beam is shown in Fig. 5. The estimated accuracy of each divergence measurement is better than 90%. A divergent laser beam allows the beam waist to

be much greater than the sample, but the divergence of the incident wave may affect the scattered pattern. Also, a diverging beam will saturate the far forward detectors unless a circular hole is placed to limit the size of the spot, but this hole introduces diffraction rings, which interferes with the expected scattering pattern. A convergent beam, which reduces the size of the beam waist, produces results that differ greatly from that expected with plane waves. A laser beam with a waist approximately equal to the size of the sphere produces diffraction rings as seen in Fig. 5 (the negative divergent condition), which are expected (Colak et al. 1979). Comparing these results to those presented in the beam diameter study, it is seen that, as long as the beam diameter is not the same as the diameter at the sphere, the effects are similar, that is, a higher beam divergence produces the same effect as a larger beam diameter.

The pedestal is a cylinder approximately 1 mm in diameter upon which the scattering sample is glued. Though it is blackened and roughened to reduce reflections, the pedestal itself produces a scattering profile that has been measured and is seen to be at least a decade lower than the signal produced by the glass sphere at all measured angles. There is also the interaction of the pedestal with the light scattered from the scattering sample. To determine the degree of this interaction and to further determine the effect of the pedestal on the scattering results, a knife edge was positioned in the laser beam to obstruct the laser beam's extent on the pedestal and sphere, as seen in the upper cartoon of Fig. 6. The incident laser beam has a beam waist of approximately 8 mm and is linearly polarized perpendicular to the scattering plane. Results obtained with the laser polarized parallel to the scattering plane are similar.

The differences between the signals retrieved in each of these four cases are less than 10%, but there is a definite trend toward a better fit, as determined by a least squares difference, to the theoretical expectations as the knife edge obscures the pedestal. The knife edge in case 4 partially shields the sphere from the incident laser beam; the goal is to reduce the effect of interaction between the sphere and the pedestal. This resulted in a better fit to expectations. The experimental result between $\theta = 90°$ and 155° is higher than the theoretical prediction because of the light scattered into the forward direction is reflected back into the reverse direction by experimental equipment in its path. Beam stops are used to reduce this effect. These results indicate that the pedestal has an effect on the retrieved scattering signal, but it is much less than the signal from the sample under study. To reduce the pedestal signal, we ensure that the sample occupies most of the laser beam profile, and minimize the extent of the pedestal into the beam. The amount that the sample interacts with the pedestal is not known at this time, but it is minimized by keeping the sample size much larger than the pedestal. Both of these conditions requires that we configure the incident laser beam diameter as large as possible.

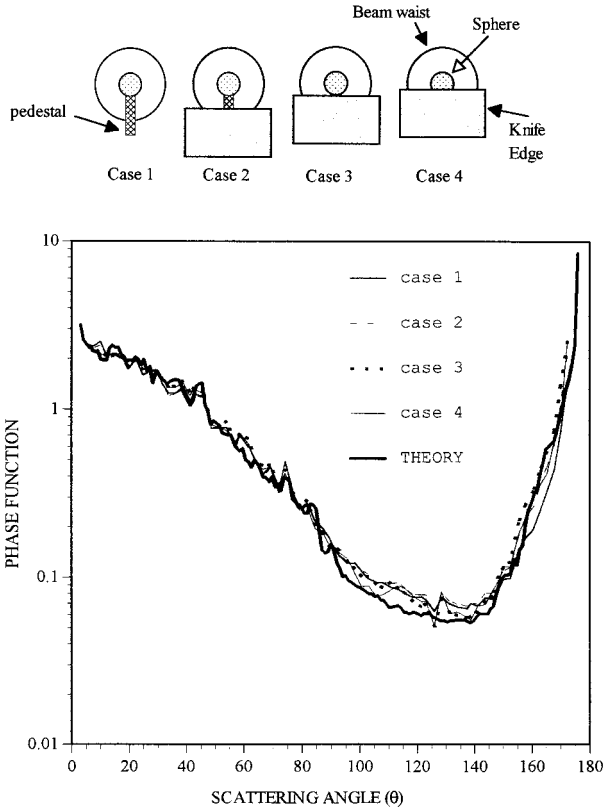

FIG. 6. Effect of increased shielding of the mounting pedestal on the light scattering characteristics of a 5-mm glass sphere.

b. Infinite cylinder

A scattering sample that avoids some of the experimental problems encountered with the sphere is the infinite cylinder. The top of Fig. 7 shows the configuration used to simulate an infinite cylinder in the experiment. The cylinder is mounted without a pedestal or any other mounting hardware intruding into the incident laser beam. The cylinder is chosen with a diameter much smaller than the incident laser beam waist size, therefore the scattering effects due to the Gaussian aspect of the laser beam are avoided.

The exact solution to the scattering characteristics of this configuration has been known since 1918 (Rayleigh 1918) and has been experimentally measured by many researchers (i.e., Kodis 1952). The exact solutions calculated for this experiment are smoothed to reflect the experimental conditions in a manner similar to that used on the Mie solution to the scattering properties of the sphere.

The cylinder studied is a fused silica fiber originally designed for optical communication. It has an index of refraction of 1.457 02, negligible absorption, and a diameter of 600 μm. A length of fiber 10 cm long is self-supporting when it is placed on its end and is mounted to the small precision tilt table such that a section of the fiber is illuminated by the complete laser beam spot.

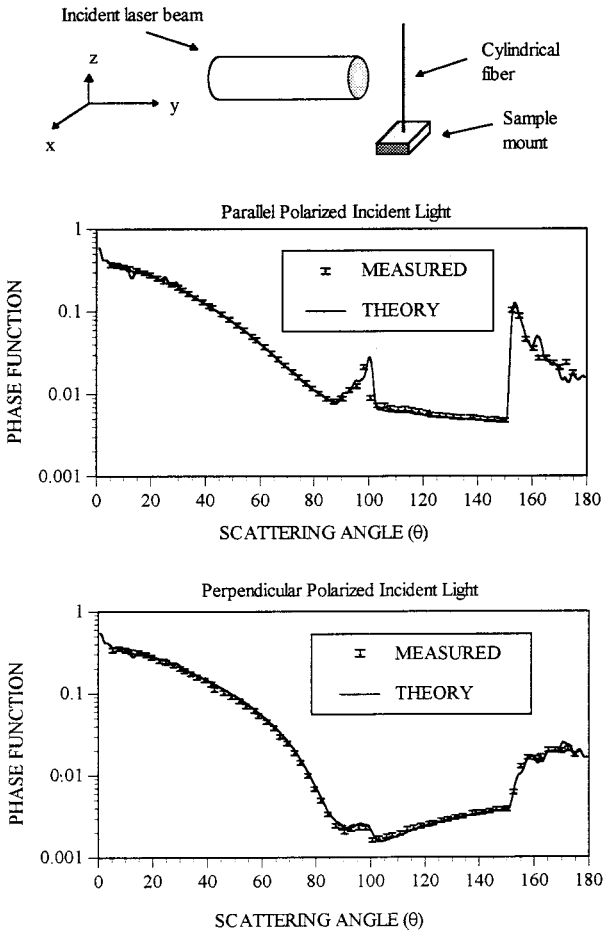

FIG. 7. Experimentally and theoretically produced phase functions for an infinite cylinder (index of refraction = 1.457) with incident helium neon laser light polarized perpendicular (middle) and parallel (bottom) to the scattering plane. The experimental arrangement is shown at the top of the figure.

The laser beam waist size is approximately 7 mm, which is much greater than the sample diameter. Colak et al. (1979) determined that if a TEM_{00} laser beam waist is five times greater than the diameter of a sphere, the resulting scattering pattern would deviate less than 5% from that produced by an incident plane wave. It is assumed that this also holds true for cylinders. Also, the variation in intensity of the incident laser beam over this scattering sample at the laser beam center due to the Gaussian aspect of the laser beam is less than 0.4%.

In Fig. 7 is shown the angular scattering intensity produced by helium neon laser light linearly polarized perpendicular (middle plot) and parallel (bottom plot) to the scattering plane incident on the quartz cylinder. There are 6% error bars on the experimental results as previously discussed. The two peaks seen at the angles of 150° and 100° are the first and second rainbow peaks similar to those produced by a sphere. The oscillations in the pattern seen just outside of these peaks are due to interference of the incident light similar to the supernumerary rings produced by spheres. Between the angles of 100°–120° and the measurement at 172° the experiment is slightly higher than expected. This is probably due to forward scattered light from the cylinder reflecting off surfaces in the experiment during reverse measurements. Despite these slight differences, the experimental results agree very well with the theoretical expectations for both polarization directions.

Because the light scattered by the glass cylinder is confined to the horizontal plane, it is possible to construct beam traps to prevent unwanted light (i.e., forward scattered light during reverse measurements) from reflecting off internal instrument components and affecting the measured results. It is not possible to make beam traps to reduce this systematic error to undetectable levels when the sample scatters into three dimensions, that is, the sphere. This is seen as a greater discrepancy between the expected result and the measured result in the reverse direction for spheres (Fig. 6) than for the cylinder (Fig. 7).

5. Summary

An experimental apparatus has been built to measure the light scattering characteristics of a small scatterer at both the scattering and azimuthal directions, excluding the far forward and reverse angles. The accuracy in which the apparatus can detect scattered light has been measured and a conservative estimate of the accuracy of detection is 94%. The incident laser beam has a characteristic TEM_{00} profile. The effect of this profile on the light scattering properties of a glass sphere is shown to be significant. To compensate, the incident laser beam profile can be used in the theoretical calculations, or the laser beam waist size can be made larger than the sample being studied.

The effect of the size of the laser beam, the convergence of the laser beam and the effects of the sample mount have all been measured using a small glass sphere. In order to produce comparable experimental results, the incident laser beam must be collimated. An incident laser beam diameter of approximately 22 mm is optimal for this experiment. The sample mount is painted with a black, nonreflective paint and is shielded to reduce its effect on the measured scattering intensities. The sample size must be as large as possible to minimize the effect of the sample pedestal. Light scattered by the sample can be reflected off the experimental apparatus and back into the photodiode array, which produces unusual and undesired light signals particularly when making reverse scattering measurements. Each scattering sample produces its own forward scattering characteristics, therefore beam traps are required for each sample.

A glass fiber oriented to produce the two-dimensional scattering intensities of an infinite cylinder has been measured by this apparatus. This sample avoids problems associated with the Gaussian laser beam profile

and the sample mount. The experimentally measured light scattered from this sample with incident light polarized parallel and perpendicular to the scattering plane compare very well with theoretical expectations. Methods have been developed to accurately measure the light scattering properties of a small sample with this apparatus. In Part II of this paper, the light scattering properties of ice like particles will be presented.

Acknowledgments. This research was supported by NSF Grant ATM-93-15251. The theoretical calculations in this paper have been kindly provided by Drs. Y. Takano and P. Yang. B. Zhang helped with the construction of the apparatus.

REFERENCES

Barkey, B., 1997: An analog light scattering experiment of hexagonal ice-like crystals. Ph.D. thesis, University of Utah, Salt Lake City, 161 pp.

Budde, W., 1979: Multidecade linearity measurements on Si photodiodes. *Appl. Opt.,* **18,** 1555–1558.

Colak, S., C. Yeh, and L. W. Casperson, 1979: Scattering of focused beams by tenuous particles. *Appl. Opt.,* **18,** 294–302.

Dugin, V. P., O. A. Volkovitskiy, S. O. Mirumyants, and N. K. Nikiforova, 1977: Anisotropy of light scattered by artificial crystalline cloud formations. *Izv. Atmos. Ocean. Phys.,* **13,** 22–25.

Eppeldauer, G., and J. E. Hardis, 1991: Fourteen-decade photo current measurements with large-area silicon photodiodes at room temperature. *Appl. Opt.,* **30,** 3091–3099.

Fuller, K. A., G. L. Stephens, and B. D. Jersak, 1994: Some advances in understanding light scattering by nonspherical particles. *Proc. Eighth Conf. on Atmospheric Radiation,* Nashville, TN, Amer. Meteor. Soc., 319–321.

Greenberg, J. M., 1960: Scattering by nonspherical particles. *J. Appl. Physics*, **31,** 82–84.

Hage, J. I., M. Greenberg, and R. T. Wang, 1991: Scattering from arbitrarily shaped particles: Theory and experiment. *Appl. Opt.,* **30,** 1141–1152.

Huffman, P. J., and W. R. Thursby, 1969: Light scattering by ice crystals. *J. Atmos. Sci.,* **26,** 1073–1077.

Kodis, R. D., 1952: Diffraction measurements at 1.25 centimeter. *J. Appl. Phys.*, **23,** 249–255.

Kuik, F., 1992: Single scattering of light by ensembles of particles with various shapes. Ph.D. thesis, Vrije Universiteit, Amsterdam, the Netherlands, 138 pp.

Lind, A. C., R. T. Wang, and J. M. Greenberg, 1965: Microwave scattering by nonspherical particles. *Appl. Opt.,* **4,** 1555–1561.

Liou, K. N., 1992: *Radiation and Cloud Processes in the Atmosphere: Theory, Observation and Modeling.* Oxford University Press, 487 pp.

——, and Y. Takano, 1994: Light scattering by nonspherical particles: Remote sensing and climatic implications. *Atmos. Res.,* **31,** 271–298.

Pluchino, A., 1986: Observations of halo scattering from single ice crystals. *Opt. Lett.,* **11,** 276–278.

——, 1987: Scattering photometer for measuring single ice crystals and evaporation and condensation rates of liquid droplets. *J. Opt. Soc. Amer. A,* **4,** 614–620.

Rayleigh, J., 1918: The dispersal of light by a dielectric cylinder. *Philos. Mag. S.,* **36,** 365–376.

Sassen, K., and K. N. Liou, 1979a: Scattering of polarized laser light by water droplet, mixed phase and ice crystal cloud. Part I: Angular scattering patterns. *J. Atmos. Sci.,* **36,** 852–861.

——, and ——, 1979b: Scattering of polarized laser light by water droplet, mixed phase and ice crystal cloud. Part II: Angular depolarization and multiple-scattering behavior. *J. Atmos. Sci.,* **36,** 838–851.

Schuerman, D. W., R. T. Wang, B. A. S. Gustafson, and R. W. Schaefer, 1981: Systematic studies of light scattering. 1: Particle shape. *Appl. Opt.,* **20,** 4039–4050.

Takano, Y., and K. N. Liou, 1989: Solar radiative transfer in cirrus clouds. Part I: Single-scattering and optical properties of hexagonal ice crystals. *J. Atmos. Sci.,* **46,** 3–19.

——, and ——, 1995: Radiative transfer in cirrus clouds. Part III: Light scattering by irregular ice crystals. *J. Atmos. Sci.,* **52,** 818–837.

Zerrull, R. H., B. A. S. Gustafson, K. Schulz, and E. Theile-Corbach, 1993: Scattering by aggregates with and without an absorbing mantle: Microwave analog experiments. *Appl. Opt.,* **32,** 4088–4100.